Photosynth Res (2017) 134:251–263
DOI 10.1007/s11120-016-0332-0

ORIGINAL ARTICLE

Gallium ferredoxin as a tool to study the effects of ferredoxin binding to photosystem I without ferredoxin reduction

Clara Mignée[1] · Risa Mutoh[2] · Anja Krieger-Liszkay[1] · Genji Kurisu[2] · Pierre Sétif[1]

Received: 7 November 2016 / Accepted: 27 December 2016 / Published online: 15 February 2017

Abstract Reduction of ferredoxin by photosystem I (PSI) involves the [4Fe–4S] clusters F_A and F_B harbored by PsaC, with F_B being the direct electron transfer partner of ferredoxin (Fd). Binding of the redox-inactive gallium ferredoxin to PSI was investigated by flash-absorption spectroscopy, studying both the $P700^+$ decay and the reduction of the native iron Fd in the presence of Fd_{Ga}. Fd_{Ga} binding resulted in a faster recombination between $P700^+$ and $(F_A, F_B)^-$, a slower electron escape from $(F_A, F_B)^-$ to exogenous acceptors, and a decreased amount of intracomplex Fd_{Fe} reduction, in accordance with competitive binding between Fd_{Fe} and Fd_{Ga}. [Fd_{Ga}] titrations of these effects revealed that the dissociation constant for the PSI:Fd_{Ga} complex is different whether (F_A, F_B) is oxidized or singly reduced. This difference in binding, together with the increase in the recombination rate, could both be attributed to a *c.* −30 mV shift of the midpoint potential of (F_A, F_B), considered as a single electron acceptor, due to Fd_{Ga} binding. This effect of Fd_{Ga} binding, which can be extrapolated to Fd_{Fe} because of the highly similar structure and the identical charge of the two Fds, should help irreversibility of electron transfer within the PSI:Fd complex. The effect of Fd binding on the individual midpoint potentials of F_A and F_B is also discussed with respect to the possible consequences on intra-PSI electron transfer and on the escape process.

Keywords Photosynthesis · Cyanobacteria · Electron transfer · Recombination reaction · Electron escape · Redox potential · Ferredoxin binding · Photosystem I inhibitor

Abbreviations

E_m	Midpoint potential
ET	Electron transfer
F_A, F_B, F_X	The three [4Fe–4S] clusters of photosystem I
Fd	Ferredoxin
Fd_{Fe}	Iron ferredoxin
Fd_{Ga}	Gallium-substituted ferredoxin
FNR	Ferredoxin-$NADP^+$-oxidoreductase
FNR_S	The short isoform of ferredoxin-$NADP^+$-oxidoreductase
K_d	Dissociation constant
K_{d_ox}	Dissociation constant of the PSI:Fd complex when (F_A, F_B) is oxidized
K_{d_red}	Dissociation constant of the PSI:Fd complex when (F_A, F_B) is singly reduced
k_e	Rate of electron escape from $(F_A, F_B)^-$
k_r	Rate of recombination between $P700^+$ and $(F_A, F_B)^-$
k_{on}	Association rate constant
k_{off}	Dissociation rate constant
PhQ_A, PhQ_B	The two phylloquinone acceptors of photosystem I
PSI	photosystem I
PSI:Fd	Complex between photosystem I and ferredoxin
P700	Reaction center P700 chlorophyll of photosystem I

Electronic supplementary material The online version of this article (doi:10.1007/s11120-016-0332-0) contains supplementary material, which is available to authorized users.

✉ Pierre Sétif
pierre.setif@cea.fr

[1] Institut de Biologie Intégrative de la Cellule (I2BC), IBITECS, CEA, CNRS, Univ. Paris-Saclay, F-91198, Gif-sur-Yvette cedex, France

[2] Institute for Protein Research, Osaka University, Suita, Osaka 565-0871, Japan

Syn. 6803 *Synechocystis* sp. PCC6803
Th. elong. *Thermosynechococcus elongatus*

Introduction

Photosystem I (PSI) is a light-dependent oxidoreductase which oxidizes plastocyanin or cytochrome c_6 on the lumenal side of the thylakoid membrane and reduces ferredoxin (Fd) or flavodoxin on its stromal side (Grotjohann and Fromme 2005; Jensen et al. 2007). Photoinduced charge separation and stabilization in PSI eventually leads to the formation of $P700^+$, a dimer of chlorophyll *a* molecules, and $(F_A, F_B)^-$, F_A and F_B being [4Fe–4S] clusters harbored by the PsaC subunit of PSI (Golbeck 2003). The core of PSI exhibits pseudo C_2-symmetry and supports double-branched electron transfer (ET) involving the two phylloquinones PhQ_A and PhQ_B in the A- and B-branches, respectively (Srinivasan and Golbeck 2009). The [4Fe–4S] cluster F_X, which is located at the pseudo-symmetry axis, is reduced by the reduced phylloquinones whereas the final steps of ET involve sequentially F_X, F_A, and F_B (Diaz-Quintana et al. 1998; Vassiliev et al. 1998). Cluster F_B is the redox partner of Fd, a soluble highly acidic 11 kDa protein with a [2Fe–2S] cluster (Fukuyama 2004). Reduced Fd must then dissociate from PSI before it can transfer an electron to a number of partners that are essential for assimilatory pathways of chloroplasts and cyanobacteria (Knaff 1996).

Crystal structures of PSIs (Amunts et al. 2010; Jordan et al. 2001) and Fds (references in Mutoh et al. 2015) have been reported whereas the structure of the PSI:Fd complex is not available yet. Moreover the X-ray structure of a gallium-substituted Fd (Fd_{Ga}) containing a [2Ga–2S] has been recently obtained and was found to be highly similar to the structure of the natural iron protein Fd_{Fe} (Mutoh et al. 2015). Fd_{Ga} is diamagnetic, contrary to Fd_{Fe}, and this property has been used to identify the different Fd residues involved in the interaction with PSI and ferredoxin-$NADP^+$-oxidoreductase (FNR) by NMR (Mutoh et al. 2015).

Functional studies by flash-absorption spectroscopy of Fd reduction by PSI have revealed kinetic complexity with several phases of intracomplex ET (Sétif and Bottin 1995), the origin of which is not clear (Sétif 2001). These studies also revealed the involvement of the 3 stromal PSI subunits, PsaC, PsaD, and PsaE, in Fd binding (references in Sétif et al. 2002). However, the dependence of the Fd to PSI-binding parameters (dissociation constants K_d) upon the redox states of PSI and Fd is not known. A better knowledge in this area is necessary to understand the energetics of complex formation and intracomplex ET and in fine to characterize Fd turnover.

In this work with flash-absorption spectroscopy, we used the property of Fd_{Ga} to be redox-inactive for probing selectively the effects of its binding to PSI in the absence of ET. Fd_{Ga} was prepared using Fd_{Fe} from *Thermosynechococcus elongatus* (*Th. elong*., Mutoh et al. 2015) and was tested with cyanobacterial PSIs from *Th. elong*. and *Synechocystis* sp. PCC6803 (*Syn*. 6803). It is shown that the detailed characterization of these effects can teach us thermodynamic and kinetic information about the "real" system with Fd_{Fe} by extrapolating the effects of Fd_{Ga} binding without ET to the effects of Fd_{Fe} binding before ET. We thus used a non-functional protein to get insight into the functional PSI/Fd system.

Materials and methods

Biological materials

Fd_{Fe} and Fd_{Ga} from *Th. elong*. were prepared as previously described (Mutoh et al. 2015). Fd_{Fe} from *Syn*. 6803 was purified as previously described (Barth et al. 2000). All PSIs were purified as previously described (Kruip et al. 1993), in the trimeric form for WT from both cyanobacteria and in the monomeric form for the PSI $E105Q_{PsaD}$ mutant (Bottin et al. 2001). The PSI and Fd concentrations were estimated by assuming absorption coefficients of 7.7 mM^{-1} cm^{-1} for $P700^+$ at 800 nm (Cassan et al. 2005) and 9.7 mM^{-1} cm^{-1} at 422 nm (Tagawa and Arnon 1968), respectively. Except where specifically indicated, measurements were made with PSI from *Th. elong*. The calculation of the concentration of colorless *Th. elong*. Fd_{Ga} was obtained from the titration of absorption changes due to Fd:FNR complex formation (Figures SI1/2), from which an absorption coefficient of 5.1 $mM^{-1}cm^{-1}$ at the 277 nm maximum was determined.

In vitro flash-absorption spectroscopy

Laser flash-induced absorption change measurements were made at 22 °C and at pH 8 in open 1-cm square cuvettes (aerobic conditions) as previously described (Sétif 2015). $P700^+$ decay was studied at 800 nm, where $P700^+$ from cyanobacterial PSI absorbs maximally in the infra-red region (Cassan et al. 2005). Most measurements of Fd reduction were made at 580 nm, a wavelength which has been extensively used in previous studies (Sétif and Bottin 1994, 1995). This wavelength has two advantages: (a) PSI has a weak absorption, which allows us to avoid relatively easily the actinic effects of the measuring light; (b) it is an isosbestic point for the formation of carotenoid triplets which may obscure the absorption signals in the µs time range. Kinetics of Fd_{Fe} reduction was obtained after

subtraction of a control measurement made on a reference cuvette without Fd_{Fe} (Sétif 2015; Sétif and Bottin 1995). This subtraction procedure allows us to observe, on a short time scale, only the reduction of Fd from $(F_A, F_B)^-$ corresponding to fast PSI:Fd intracomplex ET (<300 µs after the flash). The kinetics at both wavelengths were recorded with a DC-0.3 MHz bandwidth. This leads to some distortion of the fast subµs kinetics of Fd reduction at 580 nm (Fig. 1). All flash measurements were performed in Tricine 20 mM pH 8.0, in the presence of 5 mM $MgCl_2$, 30 mM NaCl and 0.03% β-dodecyl-maltoside, with 1 to 2.5 mM sodium ascorbate and 8 to 25 µM 2,6-dichlorophenolindophenol (DCPIP) as slow exogenous electron donors to $P700^+$.

Calculations and fits

Fd_{Fe} reduction difference signals at 580 nm were integrated between 0 and 60 µs after the flash and the integrated signals were used for data fitting. In the absence of Fd_{Ga}, a simple binding equilibrium was assumed, giving a quadratic equation in [PSI:Fd_{Fe}]. When Fd_{Ga} is present, the data were analyzed in the frame of a competitive binding model (presence of two complexes PSI:Fd_{Ga} and PSI:Fd_{Fe} exclusive one from the other), for which an exact mathematical expression is available (Wang 1995). Fits were performed using MS-Excel Solver. 3-D plots (Figure SI5) and numerical simulations (Figure SI9) were made with Mathematica 6.0.

$P700^+$ decay signals at 800 nm were fitted with 2 exponential components using Origin 7.5 (OriginLab Corp., Northampton, MA). From each biexponential fit, k_r and k_e values were calculated from Eq. (1) in Results (see also Fig. 3A). For each titration using a series of Fd_{Ga} concentrations, the initial measurement without Fd_{Ga} was used to derive k_{rF} and k_{eF}. The k_r and k_e values in the presence of Fd_{Ga} were fitted using Eqs. 3, 4 of Results and a simple binding equilibrium between Fd_{Ga} and PSI, with the three best-fit parameters k_{rC}, $k_{eC,}$ and K_{d_red}. This fit was performed using MS-Excel Solver.

Results

Fd_{Ga} inhibits reduction of Fd_{Fe} by PSI

The kinetics of Fd_{Fe} reduction by the terminal acceptor (F_A, F_B) of PSI within the PSI:Fd complex has long been studied by flash-absorption spectroscopy in the 460–600 nm region (Sétif and Bottin 1994, 1995). They are characterized by the presence of 3 different first-order components with $t_{1/2}$ of *c*. 0.5, 15, and 100 µs (Sétif 2001). During the titration of the Fd reduction signal at increasing Fd concentrations, the relative amplitudes of the three components remain constant, *i.e*., the shape of the first-order kinetics is not modified, whereas their total amplitude increases, as expected for an increase in the proportion of PSI-binding Fd. This allowed the dissociation constant K_d of the PSI:Fd complex to be calculated. Such titrations are shown in Fig. 1 at 580 nm both in the absence (part A) and the presence (0.69 µM, part B) of Fd_{Ga}, with all proteins from *Th. elong*. At a given Fd_{Fe} concentration, the signal in the presence of Fd_{Ga} is smaller than in its absence, showing that Fd_{Ga} inhibits Fd_{Fe} reduction by inhibiting the formation of the PSI:Fd_{Fe} complex. The signal amplitudes of both titrations are plotted in Fig. 1C and were fitted assuming a simple binding equilibrium between PSI and Fd_{Fe}. This resulted in $K_d = 0.74$ µM in the absence of Fd_{Ga} (red) and an apparent $K_d = 1.78$ µM in the presence of Fd_{Ga} (blue), in line with the inhibition of PSI:Fd_{Fe} complex formation by Fd_{Ga}.

The above signals are difference signals using reference cuvettes containing no Fd_{Fe} (without Fd_{Ga} for Fig. 1A and with Fd_{Ga} for Fig. 1B). It was also checked that there was no difference between the signals of the two reference cuvettes. A similar null difference recorded at a high signal-to-noise ratio is shown in Figure SI3. The absence of a Fd_{Ga}-induced signal was also checked at two other wavelengths, 480 and 540 nm, where the proportions of the 3 first-order components are different (Sétif and Bottin 1995). Such an absence of signal difference at short time due to Fd_{Ga} was *a priori* expected from the fact that Fd_{Ga} is redox-inactive. However, the possibility exists that Fd binding to PSI leads either to a change in (F_A F_B) absorption or to a change in the kinetics of ET from F_A^- to F_B, these kinetics possibly occurring in the microsecond time domain (Sétif 2001). In both cases, such a Fd-binding effect could have been mistakenly attributed to Fd reduction. The present data show that Fd_{Ga} has no such effect and this can be extrapolated to Fd_{Fe}, assuming that Fd_{Ga} and Fd_{Fe} binding to PSI have similar effects on (F_A, F_B) (as supported by data below). In turn, this implies that the fast intracomplex kinetics of Fd_{Fe} reduction is not spoiled by a signal arising from (F_A, F_B) disturbation and can be entirely attributed to Fd reduction itself.

Fd_{Ga} binds to PSI competitively with Fd_{Fe}; evidence for a single Fd-binding site in PSI

Fd_{Fe} and Fd_{Ga} have very similar structures (Mutoh et al. 2015). Moreover the [2Fe–2S] cluster of oxidized Fd_{Fe} and the [2Ga–2S] of Fd_{Ga} exhibit the same charge with metals in the +III oxidation state. Due to these similarities, it is anticipated that Fd_{Ga} binds to PSI at the same site than Fd_{Fe}, i.e., the binding is competitive. The data of Fig. 1B were fitted in a competitive binding model (exact formula from Wang 1995), by fixing the K_d for PSI:Fd_{Fe} at its

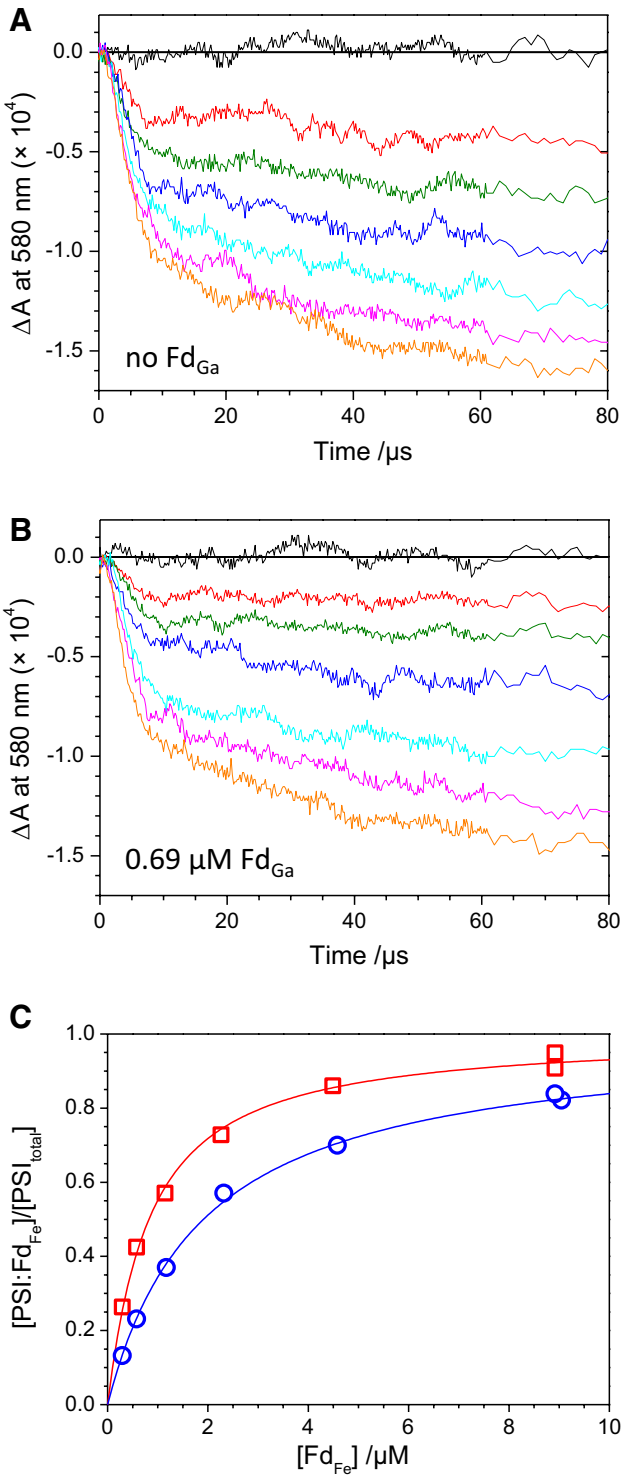

Fig. 1 Titration of the amount of PSI:Fd_{Fe} complex in the absence (**A** and *red squares* in **C**) and in the presence (**B** and *blue circles* in **C**) of Fd_{Ga}. The *signals* measured at 580 nm in **A** and **B** correspond to fast first-order intracomplex reduction of Fd_{Fe} by $(F_A, F_B)^-$ with amplitudes proportional to the amounts of PSI:Fd_{Fe} complex. These amplitudes were plotted in part **C** and fitted with models of binding equilibria. 32 measurements were averaged for each trace and a reference signal measured in the absence of Fd_{Fe} was subtracted. PSI, $Fd_{Fe,}$ and Fd_{Ga} (0.69 μM) are from *Th. elongatus*. **A** and **B**: the signal amplitudes increase with successive additions of Fd_{Fe} (0, 0.29, 0.58, 1.16, 2.29, 4.53, and 8.98 μM from *top* to *bottom* traces). PSI concentration: 0.175 μM down to 0.165 μM. Fd_{Ga} concentration: 0.69 μM down to 0.65 μM. C: the signals measured in A and B were integrated between 0 and 60 μs and the integrated signals were used to derive the proportions of PSI-binding Fd_{Fe} by best-fit analyses (*continuous curves*). Data without Fd_{Ga} (*red*) were fitted assuming a simple binding equilibrium between PSI and Fd_{Fe}, leading to $K_d(PSI:Fd_{Fe}) = 0.74$ μM. Two procedures were used to best fit the data with Fd_{Ga} (*blue*), giving superimposable curves: Firstly, a simple binding equilibrium between PSI and Fd_{Fe} led to $K_d(PSI:Fd_{Fe}) = 1.78$ μM; secondly, a competitive binding equilibrium model was used assuming a fixed $K_d(PSI:Fd_{Fe})$ of 0.74 μM, leading to $K_d(PSI:Fd_{Ga}) = 0.44$ μM

value of 0.74 μM obtained without Fd_{Ga}. The best fit was obtained for $K_d(PSI:Fd_{Ga}) = 0.44$ μM (Fig. 1C), a value almost half that of $K_d(PSI:Fd_{Fe})$. Such a two-fold difference was observed as well with two other PSI preparations from *Syn*. 6803, WT and the E105Q single-site mutation of the PsaD subunit of PSI (see Table 1). The choice of studying this mutant was made as it was found to exhibit a significant increase of its affinity for Fd (Bottin et al. 2001) and thus may be useful as a control of Fd_{Ga} binding.

Although the previous analysis with a competitive binding model gives satisfactory results, we examined further whether there could be a second Fd-binding site on PSI which may have escaped observation up to now because, *inter alia*, it was not functional for fast ET. It is anticipated that competition experiments may reveal such a secondary site if, when occupied, it modifies the properties of the functional main site by changing either the kinetics of first-order ET or the binding affinity to this site. For this purpose, we firstly compared the intracomplex kinetics of Fd_{Fe} reduction in the absence and presence of Fd_{Ga} at the three wavelengths of 480, 540, and 580 nm. We found only minor differences in the shape of the first-order kinetics which appear mostly after 80 μs after the flash (Figure SI4). Such minor differences may be attributed to the differences in the second-order diffusion-limited Fd_{Fe} reduction, the contributions of which are different whether Fd_{Ga} is present or not. Secondly we performed, by flash-absorption spectroscopy at 580 nm, competition experiments with different Fd_{Ga} concentrations of *c*. 0.34, 0.67, 1.35 μM (data in Fig. 1 are a subset of this full dataset). We also included an experiment by changing $[Fd_{Ga}]$ at a fixed Fd_{Fe} concentration of 9 μM. When globally fitting this full dataset with a competitive binding model, we obtained an almost perfect fit (Figure SI5) with $K_d(PSI:Fd_{Fe})$ and $K_d(PSI:Fd_{Ga})$ of 0.76 and 0.44 μM, respectively. Moreover, best fits of partial datasets (at fixed Fd_{Ga} concentrations or at $[Fd_{Fe}] \approx 9$ μM) with the same model gave very similar values of $K_d(PSI:Fd_{Ga})$ (between 0.40 and 0.45 μM, Figure SI6). This analysis shows that our observations are fully consistent with a competitive binding model and makes

Table 1 Dissociation constants K_ds (in μM) for binding of *Th. elong*. Fd_{Ga} and Fd_{Fe} to different PSIs

PSI	Fd	
	Th. elong. Fd_{Ga}	Th. elong. Fd_{Fe}
WT PSI *Th. elong*	**0.44**	**0.76**
WT PSI *Syn. 6803*	0.79	1.55
$E105Q_{PsaD}$ PSI *Syn. 6803*	**0.14**	**0.23**

Three different PSIs were studied: trimers from both WT strains and monomers from a *Syn*. 6803 single-site mutant (E105Q of subunit PsaD)

Numbers in bold characters are those corresponding to large datasets with the use of multiple values of $[Fd_{Ga}]$ during the competition experiments with Fd_{Fe} (Fig. SI5)

K_ds for Fd_{Fe}s were measured by titrations as the one shown in Fig. 1A, whereas K_ds for Fd_{Ga} were measured by competition experiments as those described in Fig. 1B

it unlikely that there is a second Fd bound to PSI, at least when probed with [Fd] <9 μM.

Fd_{Ga} accelerates recombination between $P700^+$ and $(F_A, F_B)^-$ and slows down electron escape from $(F_A, F_B)^-$

We studied the $P700^+$ decay following charge separation in the presence of a slow exogenous electron donor at varying Fd_{Ga} concentrations. This was measured at 800 nm on a slow time scale where two different decay components

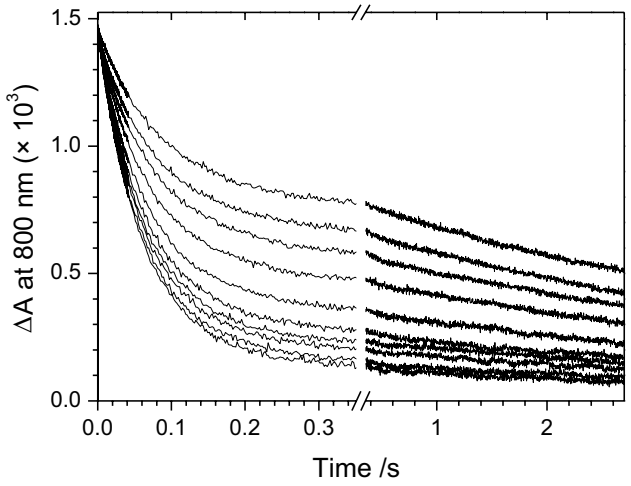

Fig. 2 $P700^+$ decay at varied Fd_{Ga} concentrations. Flash-induced absorption changes measured at 800 nm with *Th. elong*. PSI trimers. The decay accelerates with $[Fd_{Ga}]$ (0, 0.29, 0.59, 1.16, 2.32, 4.6, 6.9, 9.1, 17.9, and 35.2 μM from *top* to *bottom* trace). All kinetics were normalized to a PSI concentration of 0.19 μM (signal amplitudes corrected for dilution). Each trace is the average of 8 experiments

are observed (Fig. 2). As the Fd_{Ga} concentration increases (from top to bottom curves), the decay kinetics becomes faster and faster: the initial decay is faster and the amplitude of the faster/slower component increases/decreases with $[Fd_{Ga}]$. The biphasic decay pattern can be easily explained by the following reactions: a charge recombination (rate k_r) between $P700^+$ and $(F_A, F_B)^-$ which competes with electron escape (rate k_e) from $(F_A, F_B)^-$ to an exogenous acceptor (oxygen or another oxidized species present in the sample, see further below); when $P700^+$ is left alone without any recombination partner because of escape, it decays more slowly via reduction by the exogenous donor (rate k_{don}). The $P700^+$ decay can be easily calculated according to the previous reactions, leading to Eq. (1):

$$[P700^+(t)] = \frac{[PSI] \times k_r e^{-(k_r+k_e+k_{don})t} + k_e e^{-k_{don}t})}{(k_r + k_e)} \quad (1)$$

A kinetic example is shown in Fig. 3A, where the two exponential decay components are described in terms of rates and amplitudes. From Eq. (1), the initial $P700^+$ decay rate is:

$$\left(d[P700^+]/dt\right)(t = 0) = -\left(k_r + k_{don}\right) \times [PSI] \quad (2)$$

Equation (2) reveals that a change in the initial $P700^+$ decay rate must be attributed to a change in the recombination rate k_r (k_{don} = constant). One can then conclude from Fig. 2 that k_r increases with Fd_{Ga}. Moreover the ratio A_{fast}/A_{slow} between the amplitudes of fast and slow phases equals k_r/k_e (Eq. (1) and Fig. 3A). Whether this is due not only to an increase in k_r with $[Fd_{Ga}]$ but also to a decrease in k_e cannot be decided without a quantitative analysis done as follows. All kinetics of Fig. 2 were fitted by a biexponential decay with almost perfect fits: $P700^+(t) = [PSI]\left(A_{fast} \exp\left(-k_{fast} \times t\right) + A_{slow} \exp\left(-k_{slow} \times t\right)\right)$ with $A_{fast} + A_{slow} = 1$. K_{slow} was found to be *c*. constant, as expected from a Fd_{Ga}-independent reduction of $P700^+$ by an exogenous electron donor ($k_{slow} = k_{don}$). With the two equalities: $k_r + k_e = k_{fast} - k_{slow}$ and $A_{fast}/A_{slow} = k_r/k_e$, one can calculate k_r and k_e for each Fd_{Ga} concentration, resulting in the plots of Fig. 3B, C. These plots show that Fd_{Ga} both accelerates recombination and slows down escape.

The dissociation constant for the PSI:Fd_{Ga} complex deduced from $P700^+$ decay is larger than that found from competition experiments

The $P700^+$ decay data were further analyzed within Scheme 1. This scheme assumes that, in the presence of Fd_{Ga}, PSI can be in two states, either free or binding Fd_{Ga}, and that the recombination and escape rates of the two states differ

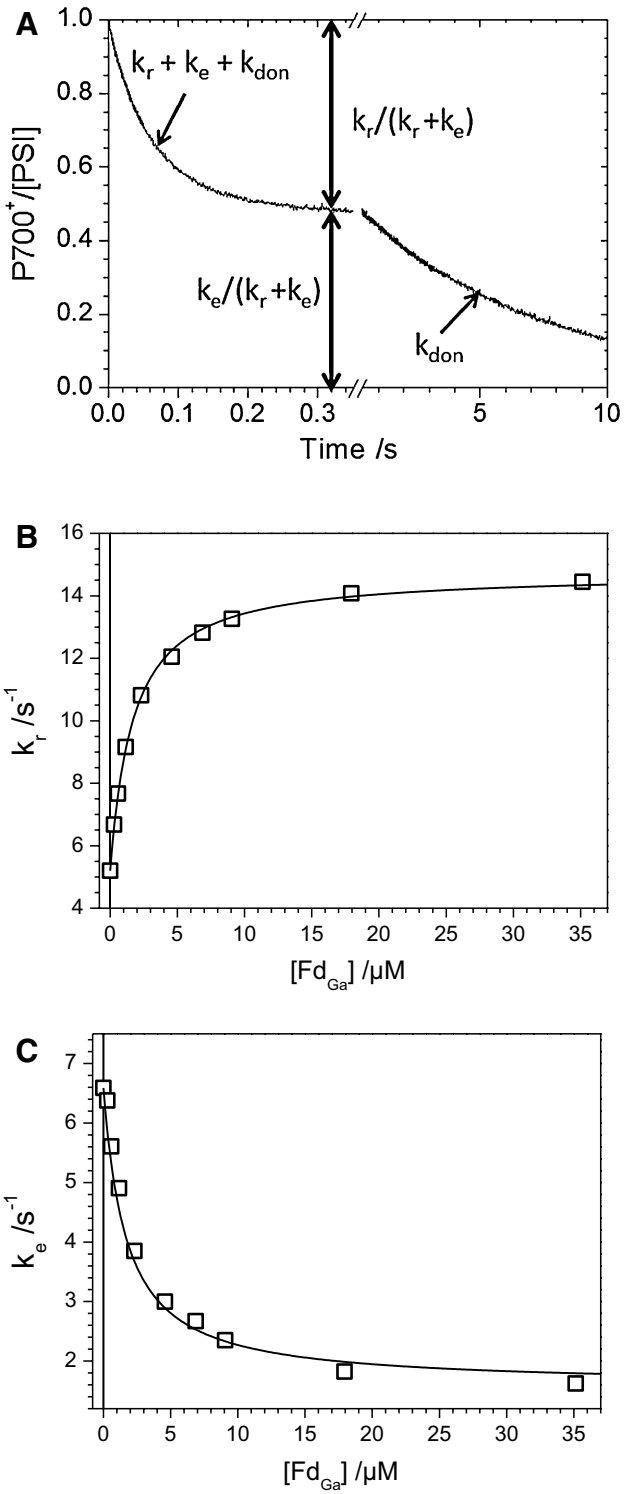

Fig. 3 Analysis of $P700^+$ decay in terms of recombination and escape process. **A**. A kinetic example is shown with rates and amplitudes of the two decaying exponential phases corresponding to Eq. (1). k_r and k_e are the recombination and escape rates, respectively, whereas k_{don} is the rate of $P700^+$ reduction by exogenous electron donors. **B** and **C**. Recombination and escape rates were calculated as a function of the Fd_{Ga} concentration after fitting each trace of Fig. 2 by a biexponential decay function and using Eq. (1). The $P700^+$ decay in the absence of Fd_{Ga} was used to derive the rates k_{rF} and k_{eF} for free PSI (5.2 and 6.6 s^{-1}, respectively). The model used to fit the kinetics in the presence of Fd_{Ga} is explained in the text and the best-fitting parameters (*continuous lines*) are the following: $k_{rC} = 14.9\ s^{-1}$, $k_{eC} = 1.4\ s^{-1}$, $K_{d\_red} = 1.45\ \mu M$

($k_{rF(free)}$ and $k_{rC(omplex)}$, $k_{eF(free)}$ and $k_{eC(omplex)}$). Moreover it was assumed in our analysis that the binding equilibrium K_{d_red} ("red" indicates that (F_A, F_B) is singly reduced) between the two forms is fast as compared to the k_r and k_e rates. This assumption is supported by the following arguments: the second-order rate constant k_{on} of Fd_{Fe} association to PSI with $(F_A, F_B)^-$ (both proteins from *Syn*. 6803) has been previously measured at a value of $3.5\times10^8\ M^{-1}s^{-1}$ (Sétif and Bottin 1995) and a similar value has been measured for both proteins from *Th. elong*. (data not shown); if one assumes a similar value for Fd_{Ga}, the association rate is 87 s^{-1} at the lowest value of $[Fd_{Ga}]$ that was used in the experiment described in Fig. 2 (0.29 μM). Moreover, with a K_d in the μM range (see below), one can calculate a dissociation rate constant $k_{off} = k_{on}\times K_{d\ (1\ \mu M)} = 350\ s^{-1}$. These rates are much larger than the k_r and k_e rates that were calculated (Fig. 3B, C). The present system is therefore under the fast exchange regime, where the recombination and escape rates are population-averaged values of the rates corresponding to free and complexed PSI, according to the equations:

$$k_r = k_{rF} \times (\text{proportion of free PSI}) + k_{rC} \times (\text{proportion of complexed PSI}), \quad (3)$$

$$k_e = k_{eF} \times (\text{proportion of free PSI}) + k_{eC} \times (\text{proportion of complexed PSI}), \quad (4)$$

where the proportions of PSI in the two states depend on the dissociation constant K_{d_red}.

The data of Fig. 3B, C were best fitted using the above formulas (continuous curves) and gave the following best-fit parameters:

$k_{rF} = 5.2\ s^{-1}$, $k_{eF} = 6.6\ s^{-1}$, $k_{rC} = 14.9\ s^{-1}$, $k_{eC} = 1.4\ s^{-1}$, $K_{d\_red} = 1.45$ μM. This experiment was repeated another time with the same PSI preparation from *Th. elong*. and was also made with the same two types of *Syn*. 6803 PSIs that were studied for competition experiments (Tables 2, 3). In a control experiment (Figure SI7), we also observed no effect of Fd_{Ga} addition on the $P700^+$ decay with a PSI mutant having a very low affinity for Fd_{Fe} [mutant R39Q of the PsaE subunit of PSI (Barth et al. 2000)].

From these data, it appears that for *Th. elong*. PSI, Fd_{Ga} binding induces a 2.7–2.9 fold increase in k_r and a 3–5 fold decrease in k_e. Comparable effects were obtained for the 2 types of *Syn*. 6803 PSI (Table 2). Moreover, the dissociation constants K_{d_red} are 2.4 to 5.2 larger than the K_ds(PSI:Fd_{Ga}) measured from competition experiments

(3.3–3.6 larger in the case of *Th. elong*. PSI, Table 3). This apparent discrepancy in K_ds will be discussed further below.

Electron escape from $(F_A, F_B)^-$. O_2 is not the only electron acceptor

Whereas all flash-absorption experiments described above were made under aerobic conditions, we also measured $P700^+$ decay at 800 nm in the absence of Fd_{Ga} with screw-cap cuvettes after prolonged incubation and agitation of PSI samples under a N_2 atmosphere in a glove box (data not shown). The slow phase decreased in amplitude indicating that oxygen can accept electrons from $(F_A, F_B)^-$ as previously observed (Jordan et al. 1998), a reaction which may contribute to the water–water cycle/Mehler reaction (Asada 2000). However, it was impossible to completely eliminate the slow phase even after extensive incubation in nitrogen, in line with previous observations (Jordan et al. 1998; Rousseau et al. 1993). This suggests that at least one other acceptor is involved.

This was confirmed by the following observation that the slow phase amplitude increases with the amount of sodium ascorbate and DCPIP (both being added for reducing slowly $P700^+$ between two consecutive flashes), indicating that oxidized forms of ascorbate and/or DCPIP could as well accept electrons from $(F_A, F_B)^-$. The effect of ascorbate/DCPIP concentrations was carefully studied during a Fd_{Ga} titration at 800 nm with both the WT and the $E105Q_{PsaD}$ mutant of *Syn*. 6803: In Table 2, the two experiments for each of the two PSIs were made at concentrations of 1 mM ascorbate/10 µM DCPIP (first line) and 2.5 mM ascorbate/25 µM DCPIP (second line). In each case, it is observed that escape is significantly larger at the highest ascorbate/DCPIP concentrations whereas recombination is not significantly affected. Moreover the Fd_{Ga} effects (ratios of k_r and k_e) were not dependent upon the ascorbate/DCPIP concentrations, suggesting that the acceptor site is the same for both oxygen and the exogenous radical(s) and that both acceptors are similarly affected by Fd_{Ga} binding. Studying in greater detail the escape process is certainly worthwhile but is outside the main scope of the present work.

(F_A, F_B) single reduction decreases the affinity of Fd_{Ga} for PSI, meaning that Fd binding decreases the midpoint potential of (F_A, F_B)

It should be first noted that the competition experiments made at 580 nm correspond to (F_A, F_B) being oxidized (hence the notation K_{d_ox} that is used further below and in Table 3). This is illustrated by Scheme 2 where equilibrium between the three states, free PSI, PSI:$Fd_{Fe,}$ and PSI:Fd_{Ga} is established in darkness, *i.e*., with oxidized (F_A, F_B) whereas fast first-order Fd reduction (bold arrow in Scheme 2) only concerns PSI:Fd_{Fe}. When a short flash is given, Fd is reduced by $(F_A, F_B)^-$ within the complex faster than the time needed for its dissociation or for Fd association to free PSI, so that there is little possibility that the equilibrium between the three above states is substantially modified before intracomplex Fd reduction takes place (slow exchange regime).

Therefore the difference between K_d determinations at 580 and 800 nm can be attributed to the fact that they correspond to different redox states of (F_A, F_B), with the PSI:Fd_{Ga} complex being destabilized by (F_A, F_B) reduction ($K_{d\_red} > K_{d\_ox}$). This complex destabilization is thermodynamically equivalent to $(F_A, F_B)^-$ destabilization by Fd_{Ga} binding to PSI, as illustrated by the thermodynamical cycle of Scheme 3.

From this cycle, Eq. (5) can be derived, where E_{mF} and E_{mC} are the midpoint potentials for single reduction of (F_A, F_B) in the free and complexed forms of PSI, respectively.

$$\Delta E_m = E_{mC} - E_{mF} = (RT/F) \times \ln\left(K_{d\_ox}/K_{d\_red}\right) \quad (5)$$

A Fd_{Ga}-binding shift of −30 mV can hence be calculated for $E_m(F_A, F_B)$ of *Th. elong*. with values of −23 and −40 mV obtained in the cases of *Syn*. 6803 PSIs (Table 3).

The fact that K_{d_ox} and K_{d_red} are different means that the model that we used for fitting the $P700^+$ decay data is oversimplified. Indeed we assumed in our analysis, for it to be tractable, that the ratio between the two PSI populations (free/complexed) remains constant during the whole $P700^+$ decay (Eqs. 3, 4). Strictly speaking, this cannot be true if $K_{d\_ox} \neq K_{d\_red}$ and this should moreover lead to a non-purely biexponential $P700^+$ decay. Firstly, it can be noted that we obtained no evidence for a significant deviation from biexponential decay. Secondly and more importantly, we tested whether our simplifying model could lead to significant errors in the best-fit parameters resulting from our analysis. This approach, described in detail in SI (Figure SI8/9/10), shows that the relative errors made on the three parameters prone to potential errors (k_{rC}, $k_{eC,}$ and K_{d_red}) are less than 2% and in turn validates our simplified model.

The Fd_{Ga}-induced acceleration of recombination can be attributed mostly to the shift of $E_m(F_A, F_B)$

Due to the large distance between P700 and (F_A, F_B) (edge-to-edge distance ≈ 40 Å), charge recombination between $P700^+$ and (F_A, F_B) is not a direct process and involves thermal repopulation of intermediate acceptors (Brettel and Leibl 2001), most probably *via* the A-side phylloquinone PhQ_A which has a higher E_m than PhQ_B (Srinivasan and Golbeck 2009) (Scheme 4). Assuming that the two states $P700^+PhQ_A^-(F_A, F_B)$ and $P700^+PhQ_A(F_A, F_B)^-$ are

in quasi-equilibrium, the recombination rate k_r between $P700^+$ and $(F_A, F_B)^-$ depends on the free energy difference between the two radical pairs according to Eq. (6):

where k_{rPhQA} is the rate of direct recombination between

$$\begin{aligned} k_r &= k_{rPhQA} \times (\exp(\Delta G/RT)/(1 + \exp(\Delta G/RT)) \\ &= k_{rPhQA} \times (\exp(\Delta G/RT) \text{ with } \Delta G/RT << -1, \end{aligned} \quad (6)$$

$P700^+$ and PhQ_A^-

One has:

$$\Delta G = F \times \left(E_m\left(PhQ_A\right) - E_m\left(F_A, F_B\right)\right) \quad (7)$$

with $E_m(PhQ_A)$ being the midpoint potential of PhQ_A when all other acceptors are oxidized.

The negative shift ΔE_m of $E_m(F_A, F_B)$ due to Fd_{Ga} binding is therefore expected to accelerate the recombination reaction, as observed. If Fd_{Ga} has no effect on $E_m(PhQ_A)$, k_{rPhQA} is not modified by Fd_{Ga} binding and, from Eqs. (6) and (7), it can be easily calculated that the ratio between $k_{rF(ree)}$ and $k_{rC(omplex)}$ depends solely on ΔE_m according to Eq. (8):

$$\ln\left(k_{rF}/k_{rC}\right) = \Delta E_m/(RT/F) \Leftrightarrow \Delta E_m = (RT/F) \times \ln\left(k_{rF}/k_{rC}\right) \quad (8)$$

Comparison of Eqs. (5) and (8) then shows the following equality between ratios of recombination rates and dissociation constants:

$$k_{rC}/k_{rF} = K\text{d\_red}/K\text{d\_ox} \quad (9)$$

For easier comparison, the ratios given in Tables 2 and 3 are duplicated in Table 4 with their standard deviations. For WT PSIs from both cyanobacterial species, the 2 ratios are quite similar, although marginally higher for K_{d_red}/K_{d_ox}. This indicates that the effect of Fd_{Ga} binding on the recombination can be attributed mostly to the negative shift of $E_m(F_A, F_B)$. The case may be slightly different for the *Syn.* 6803 $E105Q_{PsaD}$ mutant as the effect on recombination appears to be smaller than that on affinity. This difference in ratios may be attributed to the fact that Fd_{Ga} binding could also have an effect on $E_m(PhQ_A)$ in the mutant (small upward arrow beside the question mark in Scheme 4). According to our data, a small negative shift of *c.* 10 mV on $E_m(PhQ_A)$ would decrease the difference between $\Delta G_{F(ree)}$ and $\Delta G_{C(omplex)}$ leading to a smaller effect on the recombination reaction.

In a control experiment made to test indirectly whether Fd_{Ga} could have additional effects on other intermediate acceptors, we also checked with 2 different PSIs (WT from *Th. elong.* and the $E105Q_{PsaD}$ mutant from *Syn.* 6803) that Fd_{Ga} binding does not modify the yield of charge separation (Figure SI11).

Discussion

Comparison of different PSIs and different Fds

In the present study, we characterized *in vitro* the effect of *Th. elong.* Fd_{Ga} addition to PSI, and compared the binding properties of Fd_{Ga} to those of Fd_{Fe}. We also extended this study to WT PSI from *Syn.* 6803, as this system was the most extensively studied in the past. Moreover we studied the $E105Q_{PsaD}$ PSI mutant from *Syn.* 6803, which exhibits a higher affinity for Fd than WT PSI (highest affinity of all cyanobacterial PSIs yet characterized; Sétif et al. 2002), with the idea that the properties of Fd_{Ga} binding might differ in that case. Indeed the mutant was the only case where Fd_{Ga} addition significantly shifts the E_m of the phylloquinone PhQ_A involved in charge recombination, in addition to the main effect on the E_m of (F_A, F_B). This effect was however smaller (≈−10 mV) than that on (F_A, F_B). Besides this, the only significant difference between the mutant and WT from *Syn.* 6803 resided in the recombination rate between $P700^+$ and (F_A, F_B) in free PSI, with a two-fold slower rate in the mutant. This suggests that recombination, and therefore most probably $E_m(F_A, F_B)$ is sensitive to the negative charge carried by E105. Apart from these effects, the mutant behavior was essentially identical to those of both WT PSIs (similar effects of Fd_{Ga} binding on recombination and escape rates; no change in the yield of charge separation).

From Table 1, it appears that Fd_{Ga} binds to PSI 1.6 to 2.0 times better than Fd_{Fe}. As Fd_{Ga} and Fd_{Fe} have very similar structures and possess the same charge, such a consistently observed difference may have two origins, either a subtle difference between the two Fd structures or a different partial charge localization within the cluster or between the cluster and the cysteine ligands.

Competitive binding of Fd_{Ga} and Fd_{Fe} vs single binding site

Conformational flexibility of the PSI:Fd complex has been invoked *e.g.*, on the basis of ET kinetics (Sétif and Bottin 1995) or of experimentally supported calculations (Cashman et al. 2014). Different Fd global orientations have even been proposed with Fd binding either to the side (Fromme et al. 1994; Jolley et al. 2005; Lelong et al. 1996; Sétif et al. 2002) or more to the top (Cashman et al. 2014; Jolley et al. 2005; Ruffle et al. 2000) of the stromal ridge made by the three extrinsic PsaC, PsaD, and PsaE subunits. From these reports, the question can be asked whether PSI can bind 2 Fds together.

The present kinetic data support competitive binding of Fd_{Ga} and Fd_{Fe} to PS I, thus making unlikely the possibility that 2 Fds can bind together to PSI. Moreover Fd_{Ga} binding

was tested with two different *Syn*. 6803 single-site-directed mutants that were previously shown to be the most strongly disturbed in Fd_{Fe} reduction: mutant R39Q of the PsaE subunit binds Fd_{Ga} very poorly, as judged by the unmodified kinetics of $P700^+$ decay (Figure SI7), in line with the strong loss of affinity for Fd_{Fe} (Barth et al. 2000); mutant E105Q of the PsaD subunit binds Fd_{Ga} with a sixfold better affinity than the WT from *Syn*. 6803, similarly to the affinity increase for Fd_{Fe} (K_{d_ox}, Table 1). These measurements with mutants also support the idea that Fd_{Ga} and Fd_{Fe} bind to PSI in a very similar way.

Effects of Fd binding on the individual E_ms of F_A and F_B

The present results show that Fd_{Ga} binding induces a shift of −23 to −40 mV in the midpoint potential for single reduction of (F_A, F_B) ($E_m(F_A, F_B)$) in different PSIs. Assuming that the same effect occurs upon Fd_{Fe} binding, we will use in the following the notation Fd instead of Fd_{Ga}, unless inappropriate.

During the recombination reaction, the two states (F_A^-, F_B) and (F_A, F_B^-) are in fast equilibrium which allowed us to consider (F_A, F_B), as a whole, as a single electron carrier. However, forward electron transfer from F_X to F_A to F_B to Fd_{Fe} is dependent upon the individual E_ms of F_A and F_B and therefore it is useful to know the individual Fd-binding shifts of these E_ms ($\Delta E_m(F_A)$ and $\Delta E_m(F_B)$). Unfortunately, our data are not helpful in this respect, and we will discuss this topic below only to highlight the range of possibilities compatible with both the present state of knowledge and our data.

As shown by the equations given in SI, $\Delta E_m(F_A, F_B)$ will depend upon $\Delta E_m(F_A)$ and $\Delta E_m(F_B)$ but also on the difference in E_ms of F_A and F_B in free PSI ($\Delta E_{mBA} = E_m(F_B) - E_m(F_A)$). It will be supposed in the following that F_A is the cluster of highest E_m in free PSI, in line with most titration experiments by EPR, a technique which allows F_A^-, F_B^-, and (F_A^-, F_B^-) to be distinguished (Evans et al. 1974; Heathcote et al. 1978; Ke et al. 1973). In these reports, $E_m(F_A)$ was *c*. −550 mV, while the second reduction corresponding to the state (F_A^-, F_B^-) was titrated at $E_m \approx -590$ mV. This E_m is that of F_B reduction when F_A is prereduced and is not $E_m(F_B)$ that we are presently interested in (F_B reduction with oxidized F_A; redox couple (F_A, F_B)/(F_A, F_B^-)). Because of their close proximity, it is extremely likely that the interaction potential between F_A and F_B (shift of $E_m(F_B)$ due to reduction of F_A) is significant and may be even larger than ΔE_{mBA}. If mostly of electrostatic nature, this interaction potential should be negative and could account for up to −40 mV between the two titration waves measured by EPR. In summary, this means that $E_m(F_B)$ has never been measured but it can be conservatively assumed that $E_m(F_B)$ is lower than $E_m(F_A)$ by a value comprised between a few mV and 40 mV. The difference between $E_m(F_A, F_B)$ and $E_m(F_A)$ is thus plotted in Fig. 4A as a function of ΔE_{mBA}, with ΔE_{mBA} comprised between −40 and 0 mV (equation (X) given in SI). $E_m(F_A, F_B)$ is therefore above $E_m(F_A)$ by an amount which is comprised between 5 mV (when $E_m(F_B)$ is 40 mV lower than $E_m(F_A)$) and 18 mV (entropy-like factor of $(RT/F) \times \ln(2)$) when $E_m(F_B) = E_m(F_A)$.

In Fig. 4B, we plotted curves corresponding to the couple of [$\Delta E_m(F_A)$, $\Delta E_m(F_B)$] values which gives $\Delta E_m(F_A, F_B) = -30$ mV, as found with *Th. elong*. PSI, with the different curves corresponding to different ΔE_{mBA} values between −40 and 0 mV. We also assumed that $\Delta E_m(F_A)$ and $\Delta E_m(F_B)$ are comprised between −60 mV and 0 mV. All curves cross at a single point (−30 mV, −30 mV), as expected from the fact that identical shifts on $E_m(F_A)$ and $E_m(F_B)$ should shift $E_m(F_A, F_B)$ by the same value. With $\Delta E_{mBA} = 0$ (F_A and F_B of identical E_m in free PSI, black curve in Fig. 4B), couples of values are symmetrically distributed across the diagonal, meaning that there is no preferential influence of $\Delta E_m(F_A)$ or $\Delta E_m(F_B)$ on $\Delta E_m(F_A, F_B)$. By contrast, when $E_m(F_B)$ is well below $E_m(F_A)$, the range of $\Delta E_m(F_B)$ values is larger than the range of $\Delta E_m(F_A)$ values. This means that ΔE_{mBA} is mainly determined by $\Delta E_m(F_A)$ or in other words, that a given shift of $E_m(F_A)$ has a larger effect on $\Delta E_m(F_A, F_B)$ than a similar shift of $E_m(F_B)$.

What could be the respective effects of Fd binding on $E_m(F_A)$ and $E_m(F_B)$? As F_B is closer to the PSI surface than

Scheme 1 Reactions involved in the decay of the charged pair $P700^+$ (F_A, F_B)$^-$ with PSI-binding or -not-binding Fd_{Ga}

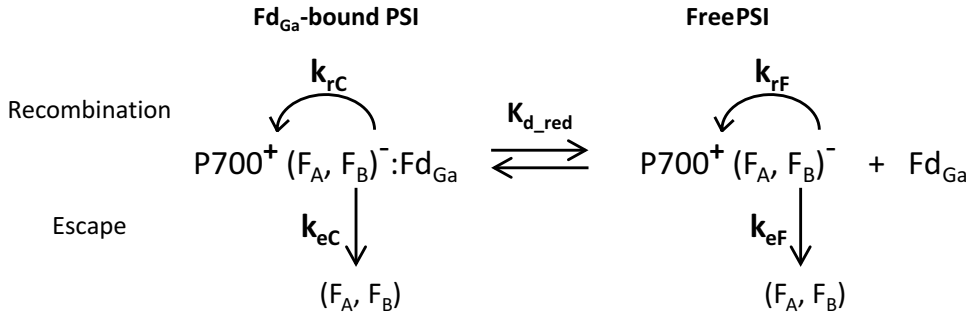

Table 2 Effect of Fd_{Ga} addition on the kinetic characteristics of $P700^+$ decay in isolated PSI (Figs. 2, 3, Eqs. 1, 3, 4)

	Free PSI		Complexed PSI PSI:Fd_{Ga}		Ratio of rates (complexed PSI/ free PSI)	
	Recomb. k_{rF}/s^{-1}	Escape k_{eF}/s^{-1}	Recomb. k_{rC}/s^{-1}	Escape k_{eC}/s^{-1}	Recomb. k_{rC}/k_{rF}	Escape k_{eC}/k_{eF}
WT PSI *Th. elong.*	5.2	6.6	14.9	1.4	2.9	0.21
	5.3	5.0	14.1	1.5	2.7	0.30
WT PSI *Syn. 6803*	8.3	4.9	19.5	1.0	2.35	0.20
	8.5	7.7	19.2	1.5	2.3	0.19
E105Q_{PsaD} PSI *Syn. 6803*	4.1	5.2	13.3	1.8	3.25	0.35
	4.7	9.5	14.6	3.3	3.1	0.35

For both PSIs from *Syn.* 6803, the experiments corresponding to the first and second line were made with (1 mM sodium ascorbate, 10 µM DCPIP) and (2 mM sodium ascorbate, 25 µM DCPIP), respectively

Concentrations were not adjusted precisely in the case of PSI from *Th. elong*

Table 3 Properties of Fd_{Ga} binding to photosystem I, characterized with (F_A, F_B) being either oxidized or singly reduced

	580 nm K_{d_ox} (Fd_{Ga})/µM	800 nm K_{d_red}(Fd_{Ga})/(µM)	Ratio K_{d_red}(Fd_{Ga})/ K_{d_ox}(Fd_{Ga})	E_m shift due to Fd_{Ga} binding/ mV
WT PSI *Th. elong*	0.44	1.45	3.3	−30
		1.57	3.6	−32
WT PSI *Syn. 6803*	0.79	2.09	2.6	−24
		1.91	2.4	−22
E105Q_{PsaD} PSI *Syn. 6803*	0.14	0.72	5.2	−42
		0.63	4.4	−38

K_ds (in µM) were measured either at 580 nm, with oxidized (F_A, F_B) (K_{d_ox}, values from Table 1) or at 800 nm, with singly reduced (F_A, F_B) (K_{d_red}). K_{d_red}s were obtained from the series of kinetics as in Fig. 2

Scheme 2 Fd_{Fe} fast reduction (*thick arrow*) occurring from a preestablished dark equilibrium involving the PSI:Fd_{Fe} and PSI:Fd_{Ga} complexes

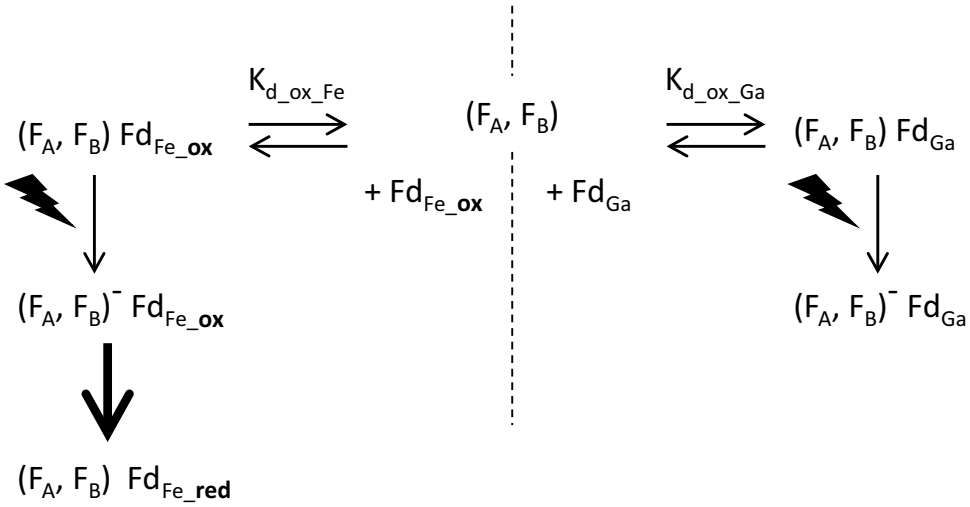

F_A (Jordan et al. 2001) and is the direct ET partner of Fd (Diaz-Quintana et al. 1998; Vassiliev et al. 1998), it can be hypothesized that it is more strongly disturbed than F_A by Fd binding ($|\Delta E_m(F_B)| > |\Delta E_m(F_A)|$), as highlighted by the hashed area in Fig. 4B. Then the "global" shift of E_m(F_A, F_B) should favor Fd reduction within the complex whereas the individual effects on E_m(F_A) and E_m(F_B) should slow down reduction of F_B from F_A^-. Fd binding would therefore make the slightly uphill ET from F_A to F_B presumably present in free PSI even more uphill. As this situation appears to be quite compatible with a high rate of Fd reduction, it means that ET from F_A to F_B is nevertheless very fast in the presence of Fd because of the small distance separating the two clusters (Sétif 2001).

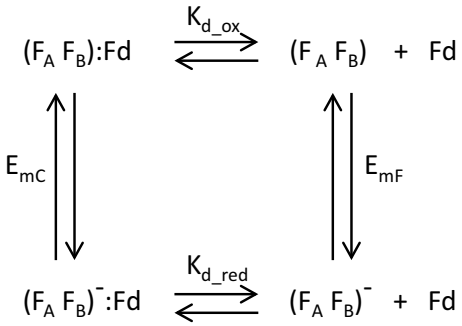

Scheme 3 Thermodynamical cycle relating Fd-binding affinities in 2 different redox states of (F_A, F_B) and midpoint potentials of (F_A, F_B) in Fd-binding *vs* Fd-non-binding states

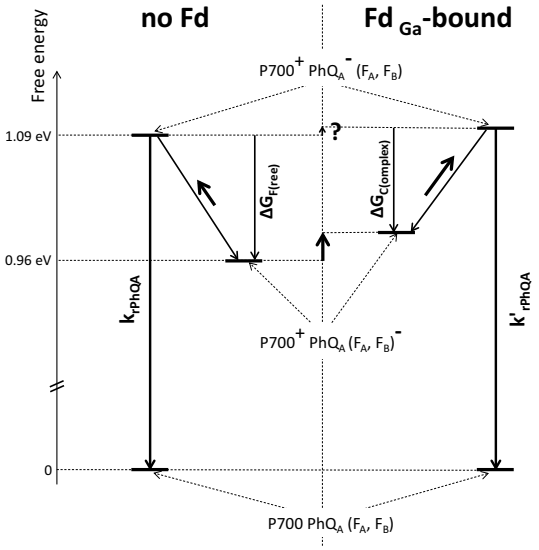

Scheme 4 Energetics and reactions involved in the recombination reaction between $P700^+$ and $(F_A, F_B)^-$ in the Fd-binding *vs* Fd-non-binding states. The free energies in eV are calculated assuming midpoint potentials of 0.42 V for $P700^+/P700$ (value for *Th. elong*., Nakamura et al. 2011), −0.54 V for $(F_A, F_B)/(F_A, F_B)^-$, and −0.67 V for PhQ_A/PhQ_A^- (Santabarbara et al. 2005)

Considering again (F_A, F_B) as a whole as a single electron carrier, the negative shift of $E_m(F_A, F_B)$ in the PSI:Fd complex should help in the irreversibility of ET between (F_A, F_B) and Fd within the complex. However, this point cannot be discussed quantitatively as long as the shift of E_m(Fd) induced by complex formation remains known. Whereas work is underway to attempt to characterize this shift, it can be noted that a negative shift of E_m(Fd) has been observed in complexes with FNR, with values ranging from −90 mV (Batie and Kamin 1981) to −22/−15 mV (Pueyo et al. 1992; Smith et al. 1981). Such a shift is in accordance with a lower solvent accessibility in the complex, as water solvation is considered to increase the midpoint potential of exposed iron–sulfur clusters (Stephens et al. 1996).

Table 4 Comparison of ratios involving either Fd_{Ga} binding for 2 different redox states of (F_A, F_B) (singly reduced *vs* oxidized) or binding-dependent recombination rates between $P700^+$ and $(F_A, F_B)^-$

	Ratio of dissociation constants K_{d_red}/K_{d_ox}	Ratio of recombination rates $k_{rComplex}/k_{rFree}$
WT PSI *Th. elong*	3.45 ± 0.21	2.8 ± 0.14
WT PSI *Syn. 6803*	2.5 ± 0.14	2.32 ± 0.04
E105Q_{PsaD} PSI *Syn. 6803*	4.8 ± 0.5	3.17 ± 0.1

The ratios are average values of those reported in Tables 2 and 3 together with their standard deviations

Effect of Fd_{Ga} binding on electron escape from (F_A, F_B)$^-$

It has been previously reported that electron escape is *c*. 10-fold smaller after selective destruction of F_B (Diaz-Quintana et al. 1998). This effect can be attributed to the fact that escape is much less efficient from F_A^- than from F_B^-. A decrease of electron escape with Fd_{Ga} binding may thus be attributed to a decreased proportion of F_B^-versus F_A^- in singly reduced (F_A, F_B), in accordance with the idea discussed above that Fd_{Ga} binding may induce a larger negative shift on $E_m(F_B)$ than on $E_m(F_A)$. However, the electron escape decrease can as well be attributed to a decreased access to oxygen (or alternative electron acceptors) in the complex. For distinguishing these two alternative possibilities, it would be *e.g*., useful to compare the [O_2] dependence of escape in PSI with and without Fd_{Ga}, a task which is outside the scope of the present study. Whatever the explanation, using Fd_{Ga} binding as a tool to limit electron escape and thus to accumulate reduced acceptors under conditions of PSI multiple turnover may prove useful to mimic, in vitro, situations where the acceptor side of PSI is overreduced in vivo.

Fd_{Ga} as an inhibitor

The present work provides clear evidence that Fd_{Ga} binding to PSI can lead to significant effects, including competitive binding with Fd_{Fe}. Fd_{Ga} can thus be considered as an inhibitor of PSI function, whose effects on PSI are not fully explored yet. It can be anticipated that the inhibitory role of Fd_{Ga} will be of great use to identify and characterize in vitro other Fd-dependent processes.

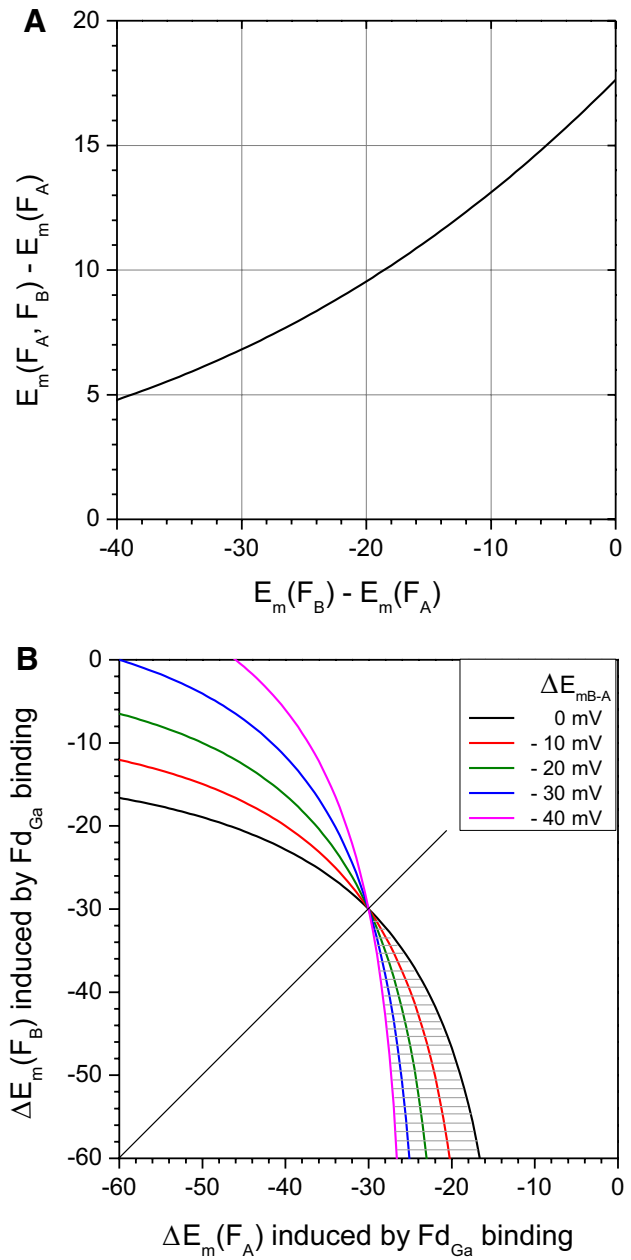

Fig. 4 Difference in midpoints potentials E_ms for the terminal PSI acceptors F_A and F_B. **A** Difference between $E_m(F_A, F_B)$ [(F_A, F_B) considered as a single electron carrier] and $E_m(F_A)$ as a function of the difference ΔE_{mBA} between the individual E_ms of F_B and F_A (equation (X) of SI). **B** Family of curves, all assuming that Fd_{Ga} binding induces a −30 mV on $E_m(F_A, F_B)$ and each one corresponding to a different value of ΔE_{mBA}. Each curve plots the Fd_{Ga}-binding-induced shift of F_B ($E_m(F_B)$) as a function of the same quantity for F_A (equation (Z) of SI)

Acknowledgements Dr. Bernard Lagoutte is thanked for his gift of purified PSI, Fd_{Fe}, and FNR_S. This work was supported by the French Infrastructure for Integrated Structural Biology (FRISBI) ANR-10-INSB-05 and by CREST, Japan Science and Technology Agency.

References

Amunts A, Toporik H, Borovikova A, Nelson N (2010) Structure determination and improved model of plant photosystem I. J Biol Chem 285:3478–3486

Asada, K (2000) The water-water cycle as alternative photon and electron sinks. Philos Trans R Soc London B 355:1419–1430

Barth P, Guillouard I, Sétif P, Lagoutte B (2000) Essential role of a single arginine of photosystem I in stabilizing the electron transfer complex with ferredoxin. J Biol Chem 275:7030–7036

Batie CJ, Kamin H (1981) The relation of pH and oxidation–reduction potential to the association state of the ferredoxin.ferredoxin:$NADP^+$ reductase complex. J Biol Chem 256:7756–7763

Bottin, H, Hanley, J, Lagoutte, B (2001) Role of acidic amino acid residues of PsaD subunit on limiting the affinity of photosystem I for ferredoxin. Biochem Biophys Res Comm 287:833–836

Brettel K, Leibl W (2001) Electron transfer in photosystem I. Biochim Biophys Acta 1507:100–114

Cashman DJ, Zhu T, Simmerman RF, Scott C, Bruce BD, Baudry J (2014) Molecular interactions between photosystem I and ferredoxin: an integrated energy frustration and experimental model. J Mol Recognit 27:597–608

Cassan N, Lagoutte B, Sétif P (2005) Ferredoxin-NADP + reductase: Kinetics of electron transfer, transient intermediates, and catalytic activities studied by flash-absorption spectroscopy with isolated photosystem I and ferredoxin. J Biol Chem 280:25960–25972

Diaz-Quintana A, Leibl W, Bottin H, Sétif P (1998) Electron transfer in photosystem I reaction centers follows a linear pathway in which iron-sulfur cluster FB is the immediate electron donor to soluble ferredoxin. BioChemistry 37:3429–3439

Evans, MCW, Reeves SG, Cammack R (1974) Determination of the oxidation–reduction potential of the bound iron-sulfur proteins of the primary electron acceptor complex of photosystem I in spinach chloroplasts. FEBS Lett 49:111–114

Fromme P, Schubert WD, Krauss N (1994) Structure of photosystem I : Suggestions on the docking sites for plastocyanin and ferredoxin, and the coordination of P700. Biochim Biophys Acta 1187:99–105

Fukuyama K (2004) Structure and function of plant-type ferredoxins. Photosynth Res 81:289–301

Golbeck, JH (2003) The binding of cofactors to photosystem I analyzed by spectroscopic and mutagenic methods. Annu Rev Biophys Biomol Struct 32:237–256

Grotjohann I, Fromme P (2005) Structure of cyanobacterial Photosystem I. Photosynth Res 85:51–72

Heathcote P, Williams-Smith DL, Sihra CK, Evans, MCW (1978) The role of the membrane-bound iron-sulfur centers A and B in the photosystem I reaction centre of spinach chloroplasts. Biochim Biophys Acta 503:333–342

Jensen PE, Bassi R, Boekema EJ, Dekker JP, Jansson S, Leister D, Robinson C, Scheller HV (2007) Structure, function and regulation of plant photosystem I. Biochim Biophys Acta 1767:335–352

Jolley C, Ben Shem A, Nelson N, Fromme P (2005) Structure of plant photosystem I revealed by theoretical modeling. J Biol Chem 280:33627–33636

Jordan, R., Nessau, U., and Schlodder, E. (1998) Charge recombination between the reduced iron-sulphur clusters and P700+. In G. Garab ed Photosynthesis: mechanisms and effects, Kluwer Academic Publishers, Dordrecht, pp. 663–666.

Jordan P, Fromme P, Witt HT, Klukas O, Saenger W, Krauss N (2001) Three-dimensional structure of cyanobacterial photosystem I at 2.5 Å resolution. Nature 411:909–917

Ke B, Hansen RE, Beinert H (1973) Oxidation–reduction potentials of bound iron-sulfur proteins of photosystem I. Proc Natl Acad Sci USA 70:2941–2945

Knaff DB (1996) Ferredoxin and ferredoxin-dependent enzymes. In D.R. Ort and C. Yocum eds Oxygenic photosynthesis: the light reactions, Kluwer Academic Publishers, Berlin, pp. 333–361

Kruip J, Boekema EJ, Bald D, Boonstra AF, Rögner M (1993) Isolation and structural characterization of monomeric and trimeric photosystem I complexes ($P700.F_A/F_B$ and $P700.F_X$) from the cyanobacterium *Synechocystis* PCC 6803. J Biol Chem 268:23353–23360

Lelong C, Boekema EJ, Kruip J, Bottin H, Rögner M, Sétif P (1996) Characterization of a redox active crosslinked complex between cyanobacterial photosystem I and soluble ferredoxin. EMBO J 15:2160–2168

Mutoh R, Muraki N, Shinmura K, Kubota-Kawai H, Lee YH, Nowaczyk MM, Rogner M, Hase T, Ikegami T, Kurisu G (2015) X-ray structure and nuclear magnetic resonance analysis of the interaction sites of the Ga-substituted cyanobacterial ferredoxin. BioChemistry 54:6052–6061

Nakamura A, Suzawa T, Kato Y, Watanabe T (2011) Species dependence of the redox potential of the primary electron donor P700 in photosystem I of oxygenic photosynthetic organisms revealed by spectroelectrochemistry. Plant Cell Physiol 52:815–823

Pueyo JJ, Revilla C, Mayhew SG, Gomez-Moreno C (1992) Complex formation between ferredoxin and ferredoxin-NADP + reductase from Anabaena PCC 7119: cross-linking studies. Arch Biochem Biophys 294:367–372

Rousseau F, Sétif P, Lagoutte B (1993) Evidence for the involvement of PSI-E subunit in the reduction of ferredoxin by photosystem I. EMBO J 12:1755–1765

Ruffle SV, Mustafa AO, Kitmitto A, Holzenburg A, Ford RC (2000) The location of the mobile electron carrier ferredoxin in vascular plant photosystem I. J Biol Chem 275:36250–36255

Santabarbara S, Heathcote P, Evans, MCW (2005) Modelling of the electron transfer reactions in photosystem I by electron tunnelling theory: The phylloquinones bound to the PsaA and the PsaB reaction centre subunits of PSI are almost isoenergetic to the iron-sulfur cluster Fx. Biochim Biophys Acta 1708:283–310

Sétif P (2001) Ferredoxin and flavodoxin reduction by photosystem I. Biochim Biophys Acta 1507:161–179

Sétif P (2015) Electron-transfer kinetics in cyanobacterial cells: Methyl viologen is a poor inhibitor of linear electron flow. Biochim Biophys Acta 1847:212–222

Sétif P, Bottin H (1994) Laser flash absorption spectroscopy study of ferredoxin reduction by photosystem I in Synechocystis sp. PCC 6803: Evidence for submicrosecond and microsecond kinetics. BioChemistry 33:8495–8504

Sétif P, Bottin H (1995) Laser flash absorption spectroscopy study of ferredoxin reduction by photosystem I: Spectral and kinetic evidence for the existence of several photosystem I-ferredoxin complexes. BioChemistry 34:9059–9070

Sétif P, Fischer N, Lagoutte B, Bottin H, Rochaix JD (2002) The ferredoxin docking site of photosystem I. Biochim Biophys Acta 1555:204–209

Smith JM, Smith WH, Knaff DB (1981) Electrochemical titrations of a ferredoxin-ferredoxin:$NADP^+$ oxidoreductase complex. Biochim Biophys Acta 635:405–411

Srinivasan N, Golbeck JH (2009) Protein-cofactor interactions in bioenergetic complexes: The role of the A_{1A} and A_{1B} phylloquinones in photosystem I. Biochim Biophys Acta 1787:1057–1088

Stephens PJ, Jollie DR, Warshel A (1996) Protein control of redox potentials of iron-sulfur proteins. Chem Rev 96:2491–2513

Tagawa K, Arnon DI (1968) Oxidation–reduction potentials and stoichiometry of electron transfer in ferredoxins. Biochim Biophys Acta 153:602–613

Vassiliev IR, Jung YS, Yang F, Golbeck JH (1998) PsaC subunit of photosystem I is oriented with iron-sulfur cluster FB as the immediate electron donor to ferredoxin and flavodoxin. Biophys J 74:2029–2035

Wang ZX (1995) An exact mathematical expression for describing competitive-binding of 2 different ligands to a protein molecule. FEBS Lett 360:111–114